Syntheses and Characterization of $W(NC_6F_5)F_5^-$ and $W_2(NC_6F_5)_2F_9^-$ Salts and Computational Studies of the $W(NR)F_5^-$ (R = H, F, CH_3, CF_3, C_6H_5, C_6F_5) and $W_2(NC_6F_5)_2F_9^-$ Anions

Douglas Turnbull[a,b], Stacey D. Wetmore[a,b], and Michael Gerken*[a,b]

[a]Canadian Centre for Research in Advanced Fluorine Technologies and [b]Department of Chemistry and Biochemistry, University of Lethbridge, 4401 University Drive W, Lethbridge, AB, CA T1K 3M4

*Corresponding author. Tel.: +1-403-329-2173; Fax: +1-403-329-2057; E-mail address: michael.gerken@uleth.ca.

Abstract

Convenient preparative routes to fluorido[(pentafluorophenyl)imido]tungstate(VI) salts have been developed. The reaction of $WF_6 \cdot NC_5H_5$ or $[N(CH_3)_4][WF_7]$ with $C_6F_5NH_2$ results in quantitative formation of the $C_5H_5NH^+$ or $N(CH_3)_4^+$ salt of the $W(NC_6F_5)F_5^-$ anion, respectively. The dissolution of $[C_5H_5NH][W(NC_6F_5)F_5]$ in anhydrous HF results in the formation of $[C_5H_5NH][W_2(NC_6F_5)_2F_9]$. These salts have been comprehensively characterized in the solid state by X-ray crystallography and Raman spectroscopy, and in solution by ^{19}F and ^{1}H NMR spectroscopy. The crystal structures of the $W(NC_6F_5)F_5^-$ salts reveal conformational differences in the anions, and the ^{19}F NMR spectra of these salts in CH_3CN reveal coupling of the axial fluorido ligand to the ^{14}N nucleus of the imido ligand. In addition, density-functional-theory (DFT-B3LYP) calculations have been performed on a series of $W(NR)F_5^-$ anions (R = H, F, CH_3, CF_3, C_6H_5, C_6F_5) and the $W_2(NC_6F_5)_2F_9^-$ anion, including gas-phase optimizations, vibrational frequencies, molecular orbitals, and natural-bond-orbital (NBO) analyses.

Introduction

Chalcogen-containing WF_6 derivatives of the form $WChF_4$ (Ch = O, S) have been known since the synthesis of WOF_4 by Ruff in 1907.[1] They form fluorine-bridged oligomeric (WOF_4) or polymeric (WSF_4) structures in the solid state,[2–4] and these aggregate species monomerize readily in the presence of a Lewis base to afford Lewis acid-base adducts.[3–12] They also behave as fluoride-ion acceptors, and the $WChF_5^-$ and $W_2Ch_2F_9^-$ anions have been characterized in the solid state and in solution.[13–18]

Analogous imidotungsten(VI) complexes of the form $W(NR)F_4$, and derivatives thereof, have also been studied (albeit more sporadically). It was first determined by ^{19}F NMR spectroscopy that the reaction of WF_6 with RNH_2 (R = H, C_4H_9) in CH_3CN affords $W(NR)F_4 \cdot NCCH_3$ if the

amine was carefully added in small amounts to the solution (eq 1), whereas $W(NR)F_5^-$ anions were observed if additional amine was introduced to the reaction mixture (eq 2).[19]

$$WF_6 + RNH_2 + CH_3CN \rightarrow W(NR)F_4 \cdot NCCH_3 + 2HF \quad (1)$$

$$WF_6 + 2RNH_2 \rightarrow [RNH_3][W(NR)F_5] + HF \quad (2)$$

The formation of $[RNH_3][W(NR)F_5]$ ($R = CH_3, C_2H_5, C_4H_9$) salts upon the reaction of WF_6 with aliphatic primary amines was also noted by Winfield and co-workers,[20,21] while the reaction of WF_6 with $CH_3NHSi(CH_3)_3$ generated a mixture of $[CH_3NH_3][W(NCH_3)F_5]$ and $[CH_3NH_3][W_2(NCH_3)_2F_9]$.[20] Alkylammonium salts were observed even when an excess of WF_6 was employed, and it was hypothesized that an intermediate $WF_6 \cdot NH_2R$ adduct is initially formed (eq 3a), which eliminates HF to form $W(NHR)F_5$ as a second intermediate (eq 3b), and the two intermediates then react to form $[RNH_3][W(NR)F_5]$ and WF_6 (eq 3c).[21]

$$WF_6 + RNH_2 \rightarrow WF_6 \cdot NH_2R \quad (3a)$$

$$WF_6 \cdot NH_2R \rightarrow W(NHR)F_5 + HF \quad (3b)$$

$$WF_6 \cdot NH_2R + W(NHR)F_5 \rightarrow [RNH_3][W(NR)F_5] + WF_6 \quad (3c)$$

The reaction of WF_6 with $C_6F_5NH_2$ in $CF_2ClCFCl_2$ was studied and several products – $C_6F_5NH_3^+$ salts of the $W(NC_6F_5)F_5^-$, $W_2(NC_6F_5)_2F_9^-$, and F^- anions – were observed in an admixture.[22] This mixture was characterized by IR spectroscopy in the solid state and ^{19}F NMR spectroscopy in CH_3CN solvent, where the $W_2(NC_6F_5)OF_9^-$ anion was also observed due to partial hydrolysis. Recrystallization of this mixture from CF_3COOH afforded $[C_6F_5NH_3][W_2(NC_6F_5)_2F_9]$ as the only tungsten-containing product, which was characterized structurally by ambient-temperature X-ray crystallography.

Analogous chloroimido complexes have been synthesized by Dehnicke and co-workers via the fluorination of $W(NCl)Cl_4$, $WNCl_3$, or the $WNCl_4^-$ anion. The reaction of $W(NCl)Cl_4$ with an alkali-metal fluoride in the presence of a crown ether led to $[Na(15\text{-crown-}5)][W(NCl)F_5]$[23] and $[K(18\text{-crown-}6)][W(NClF_5]$[24] (eq 4), whereas $K[W(NCl)F_5]$ was synthesized by the fluorination of $WNCl_3$ by a mixture of KF and $(CH_3)_3SnF$ (eq 5).[25] The fluorination of $WNCl_3$ and $W(NCl)Cl_4$ by dilute F_2 in N_2 afforded $W(NCl)F_4$.[26] The $WNCl_4^-$ anion was partially fluorinated upon reaction with $[(C_6H_5)_3C][BF_4]$, resulting in the formation of $[(C_6H_5)_3C][W_3N\{NC(C_6H_5)_3\}_2Cl_{10}F_2]$ (eq 6), in which the anion is a trinuclear complex consisting of a *trans*-$WNCl_2F_2^-$ anion coordinated to two $W\{NC(C_6H_5)_3\}Cl_4$ molecules via asymmetrical W–F···W bridges.[27] With the exception of $W(NCl)F_4$, these chloroimido complexes were characterized structurally by X-ray crystallography.

$$W(NCl)Cl_4 + 5F^- \rightarrow W(NCl)F_5^- + 4Cl^- \quad (4)$$

$$WNCl_3 + 3F^- + 2(CH_3)_3SnF \rightarrow W(NCl)F_5^- + 2Cl^- + Sn_2(CH_3)_6 \quad (5)$$

$$3WNCl_4^- + 3[(C_6H_5)_3C][BF_4] \rightarrow \quad (6)$$

$$[(C_6H_5)_3C][W_3N\{NC(C_6H_5)_3\}_2Cl_{10}F_2] + BF_4^- + 2BF_3 + 2Cl^-$$

While several fluorido(imido)tungstate(VI) complexes have been investigated previously, no single species has been isolated and comprehensively characterized. Herein, we have studied salts of the $W(NC_6F_5)F_5^-$ and $W_2(NC_6F_5)_2F_9^-$ anions, including facile preparative routes and comprehensive structural and spectroscopic characterization. In addition, the bonding within and structural properties of a series of $W(NR)F_5^-$ anions (R = H, F, CH_3, CF_3, C_6H_5), in addition to those synthesized, have been studied by density-functional-theory (DFT-B3LYP) calculations.

Results and Discussion

Syntheses and Properties of $W(NC_6F_5)F_5^-$ and $W_2(NC_6F_5)_2F_9^-$ Salts

While the reaction of WF_6 with $C_6F_5NH_2$ produces a mixture of products,[22] substituting $WF_6 \cdot NC_5H_5$ for WF_6 results in the quantitative formation of $[C_5H_5NH][W(NC_6F_5)F_5]$ (eq 7), which can then be isolated as a yellow powder by the removal of volatile materials under dynamic vacuum. This salt is highly soluble in CH_2Cl_2, CH_3CN, and SO_2.

$$WF_6 \cdot NC_5H_5 + C_6F_5NH_2 \rightarrow [C_5H_5NH][W(NC_6F_5)F_5] + HF \quad (7)$$

The $[N(CH_3)_4][W(NC_6F_5)F_5]$ salt can be isolated in a similar fashion by reacting $[N(CH_3)_4][WF_7]$ with $C_6F_5NH_2$ in SO_2 or CH_3CN solvent at ambient temperature (eq 8), followed by the removal of volatile materials under dynamic vacuum. The reaction must be conducted over several hours in SO_2 to ensure completion, though it is effectively instantaneous in CH_3CN. While thermally stable and highly soluble in CH_3CN and SO_2 like its $C_5H_5NH^+$ analog, the $N(CH_3)_4^+$ salt is insoluble in CH_2Cl_2.

$$[N(CH_3)_4][WF_7] + C_6F_5NH_2 \rightarrow [N(CH_3)_4][W(NC_6F_5)F_5] + 2HF \quad (8)$$

The $[C_5H_5NH][W(NC_6F_5)F_5]$ salt can be solvolyzed in anhydrous HF to afford $[C_5H_5NH][W_2(NC_6F_5)_2F_9]$, which contains a fluorine-bridged dinuclear $W_2(NC_6F_5)_2F_9^-$ anion (eq 9). This is analogous to previously reported preparations of $W_2Ch_2F_9^-$ salts by the solvolysis of $WChF_5^-$ anions (Ch = O, S) in anhydrous HF.[14,15,18] As with the preparation of $W_2O_2F_9^-$ salts,[14,15] the reaction exists in equilibrium, as direct removal of the anhydrous HF from the product mixture causes substantial reversion to the mononuclear anion. However, decanting the HF from the product allows for the isolation of $[C_5H_5NH][W_2(NC_6F_5)_2F_9]$ containing a small impurity of $[C_5H_5NH][W(NC_6F_5)F_5]$.

$$2\ W(NC_6F_5)F_5^- + n HF \rightleftharpoons W_2(NC_6F_5)_2F_9^- + F(HF)_n^- \quad (9)$$

The $[C_5H_5NH][W_2(NC_6F_5)_2F_9]$ salt is highly soluble in CH_3CN and SO_2, but only slightly soluble in CH_2Cl_2. At ambient temperature, the anion is partially solvolyzed by CH_3CN to afford the $W(NC_6F_5)F_5^-$ anion and $W(NC_6F_5)F_4{\cdot}NCCH_3$, as determined by ^{19}F NMR spectroscopy (eq 10).

$$W_2(NC_6F_5)_2F_9^- + CH_3CN \rightleftharpoons W(NC_6F_5)F_5^- + W(NC_6F_5)F_4{\cdot}NCCH_3 \quad (10)$$

These $W(NC_6F_5)F_5^-$ and $W_2(NC_6F_5)_2F_9^-$ salts manifest as yellow powders, forming vibrant yellow solutions that then proceed to darken to orange upon concentration under dynamic vacuum. These salts are stable at ambient temperature and highly moisture sensitive; contact with even trace amounts of moisture results in the formation of the WOF_5^- and $W_2(NC_6F_5)OF_9^-$ anions, respectively.

X-ray Crystallography

The $[C_5H_5NH][W(NC_6F_5)F_5]$, $[N(CH_3)_4][W(NC_6F_5)F_5]$, and $[C_5H_5NH][W_2(NC_6F_5)_2F_9]$ salts have been studied by X-ray crystallography at 100 K; crystallographic data collection and refinement parameters are given in Table S1 of the Supporting Information. In addition, the geometries of the $W(NC_6F_5)F_5^-$ and $W_2(NC_6F_5)_2F_9^-$ anions have been optimized using DFT methods (B3LYP), resulting in stationary points whose geometries are in excellent agreement with the crystallographic data. Selected geometric parameters (experimental and calculated) are given in Tables 1 and 2, respectively. Complete geometric parameters are given in Tables S2 and S3.

Long yellow plates of $[C_5H_5NH][W(NC_6F_5)F_5]$ were grown by cooling a CH_2Cl_2 solution to −35 °C, whereas $[N(CH_3)_4][W(NC_6F_5)F_5]$ crystallized as yellow blocks from a CH_3CN solution at −40 °C. The $C_5H_5NH^+$ salt crystallizes in the monoclinic space group $P2_1/c$ with four formula

units per unit cell and one ion pair in the asymmetric unit. The $N(CH_3)_4^+$ salt crystallizes in the orthorhombic space group *Pnma* with four formula units per unit cell and one half of an ion pair in the asymmetric unit, as the ions are reflected across *b* mirror planes. Packing diagrams are provided in the Supporting Information (Figures S1 and S2).

Table 1. Selected Experimental and Calculated Geometric Parameters for the $W(NC_6F_5)F_5^-$ Anion

	Experimental		Calculated[a]
	$C_5H_5NH^+$ Salt	$(CH_3)_4N^+$ Salt	
Bond Lengths (Å)			
W−N(1)	1.747(2)	1.755(4)	1.797
W−F(1)	2.0212(13)	1.973(3)	1.941
W−F(2)	1.8873(14)	1.8901(19)	1.898
W−F(3)	1.8770(13)	1.8866(18)	1.898
W−F(4)	1.8850(12)		1.898
W−F(5)	1.8846(14)		1.898
F(1)···N(2)	2.688(2)		
Bond Angles (°)[b]			
W−N(1)−C(1)	175.58(17)	178.5(3)	180.0
N(1)−W−F(1)	179.42(7)	179.75(15)	180.0
N(1)−W−F(2)	96.68(8)	96.57(10)	95.1
N(1)−W−F(3)	97.20(3)	95.84(10)	95.1
N(1)−W−F(4)	97.16(8)		95.1
N(1)−W−F(5)	97.65(8)		95.1
F(1)−W−F(2)	83.61(6)	83.61(9)	85.0
F(1)−W−F(3)	83.31(6)	83.98(9)	85.0
F(1)−W−F(4)	82.56(6)		85.0
F(1)−W−F(5)	81.85(6)		85.0
F(2)−W− F(2)^i/F(5)	89.63(7)	88.50(12)	89.8
F(2)−W−F(3)	87.43(7)	89.24(9)	89.8
F(2)−W− F(3)^i/F(4)	166.13(6)	167.56(8)	169.9
F(3)−W− F(3)^i/F(4)	90.03(6)	90.35(12)	89.8
F(3)−W−F(5)	165.10(7)		169.9
F(4)−W−F(5)	89.34(6)		89.8
N(2)−H(2)···F(1)	169(3)		

[a]Calculated using the B3LYP functional with the Stuttgart basis set augmented by one f-type polarization function (W; $\alpha_f = 0.823$) and *aug*-cc-pVTZ basis set (C, N, F). [b]i = +x, 1.5−y, +z.

In both $W(NC_6F_5)F_5^-$ salts, the anion adopts a pseudo-octahedral geometry (Figure 1) with the imido ligand in an axial position. In the $N(CH_3)_4^+$ salt, the W−F_{ax} bond [1.973(3) Å] is elongated relative to the W−F_{eq} bonds [1.8866(18)−1.8901(19) Å] due to a trans influence from the imido ligand. The equatorial fluorido ligands distort from the ideal WF_4 plane towards the axial

fluorido ligand due to repulsion by the imido ligand [F(1)−W−F_{eq} = 83.61(9)−83.98(9)°]. The W−N−C bond angle is approximately linear [178.5(3)°], as has been observed previously for the W−N−Cl angle in $W(NCl)F_5^-$ salts [170.7(5)−176.1(5)°].[23–25]

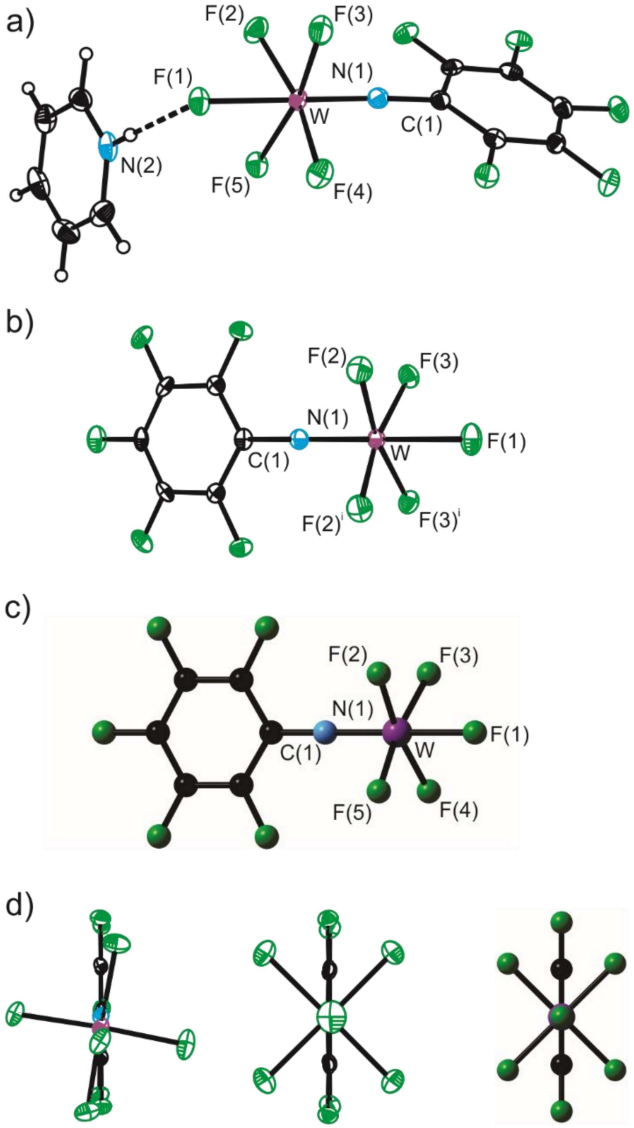

Figure 1. Geometries of the $W(NC_6F_5)F_5^-$ anion: a) thermal ellipsoid plot of $[C_5H_5NH][W(NC_6F_5)F_5]$; b) thermal ellipsoid plot of the anion in the crystal structure of $[N(CH_3)_4][W(NC_6F_5)F_5]$; c) optimized gas-phase geometry; d) end-on views of the anions from a) (left), b) (middle), and c) (right). Thermal ellipsoids are drawn at the 50% probability level.

The anion in the $C_5H_5NH^+$ salt exhibits a similar distortion of the WF_4 moiety from planarity [F(1)−W−F = 81.85(6)−83.61(6)°] and approximate linearity in the W−N−C bond angle [175.58(17)°]. The elongation of the W−F_{ax} bond [2.0212(13) Å] relative to the W−F_{eq} bonds [1.8770(13)−1.8873(14) Å] is more dramatic than in the $N(CH_3)_4^+$ salt due to N−H···F_{ax} hydrogen bonding between the cation and anion (Figure 1a); the W≡N and W−F_{eq} bond lengths are not significantly affected by this interaction. A conformational difference between the salts is also observed (Figure 1d), presumably as a result of crystal packing. In the $C_5H_5NH^+$ salt, the anion adopts a nearly eclipsed C_1 geometry, whereas in the $N(CH_3)_4^+$ salt, it adopts a staggered geometry approximating C_{2v} symmetry.

The predicted C_{2v}-symmetric gas-phase geometry is in excellent agreement with that determined crystallographically in the $N(CH_3)_4^+$ salt (Figure 1c−1d), where the primary discrepancies are a slight overestimation of the predicted W≡N bond length [1.797 vs. 1.755(4) Å] and a corresponding underestimation of the W−F_{ax} bond length [1.941 vs. 1.973(3) Å].

Extremely thin yellow plates of $[C_5H_5NH][W_2(NC_6F_5)_2F_9]$ were crystallized from a CH_3CN solution upon removal of the solvent at −40 °C. The plates were very thin and were easily fractured so that a very small crystal had to be used to acquire adequate data. The $[C_5H_5NH][W_2(NC_6F_5)_2F_9]$ salt crystallizes in the monoclinic space group *P*2/*n* with two formula units per unit cell and one half of a crystallographically unique ion pair in the asymmetric unit, as the F(1) atom is located on a twofold axis. The unit cell consists of double layers within the *ac* plane in which the cations and anions alternate along the *c* axis (Figure S3). While very weak N−H···F_{eq} hydrogen bonds are observed within the double layers, no such interactions between the double layers are observed, explaining the facile cleaving of the crystals during their selection and mounting.

Table 2. Selected Experimental and Calculated Geometric Parameters for the $W_2(NC_6F_5)_2F_9^-$ Anion

	Experimental	Calculated[a]
Bond Lengths (Å)[b]		
W−N(1)	1.724(7)	1.759
W−F(1)	2.1013(17)	2.120
W−F(2)	1.855(5)	1.883
W−F(3)	1.858(6)	1.883
W−F(4)	1.859(5)	1.883
W−F(5)	1.866(6)	1.883
F(4)···N(2)	2.958(11)	
F(3)^{j}···N(2)	3.046(13)	
F(3)^{k}···N(2)	3.082(13)	
Bond Angles (°)[c]		
W−F(1)−W^{i}	156.0(4)	180.0
W−N(1)−C(1)	176.4(6)	180.0
N(1)−W−F(1)	179.8(3)	180.0
N(1)−W−F(2)	98.6(3)	97.8
N(1)−W−F(3)	99.5(3)	97.7
N(1)−W−F(4)	98.5(3)	97.8
N(1)−W−F(5)	98.3(3)	97.7

[a]Calculated using the B3LYP functional with the Stuttgart basis set augmented by one f-type polarization function (W; $\alpha_f = 0.823$) and cc-pVTZ basis set (C, N, F). [b]j = 0.5-x, +y, 1.5-z; k = −1+x, +y, +z. [c]i = 1.5-x, +y, 0.5-z.

The $W_2(NC_6F_5)_2F_9^-$ anion adopts a bent pseudo-dioctahedral geometry with a symmetrical fluorine bridge (Figure 2) in which the W−F_{ax}−W angle [156.1(4)°] is intermediate between those observed in the $C_6F_5NH_3^+$ salt [150.8(12)−170.4(19)°]. The anion possesses crystallographically imposed C_2 symmetry and each $W(NC_6F_5)F_5$ moiety exhibits approximate C_{2v} symmetry. The C_6F_5 groups are staggered relative to the adjacent WF_4 moieties, and the WF_4 moieties are also staggered relative to one another (Figure 2b–2c), which differs from both crystallographically unique conformations observed in the $C_6F_5NH_3^+$ salt (in which the WF_4 moieties are essentially eclipsed in both cases),[22] suggesting that the conformation of the anion is highly susceptible to crystal packing effects.

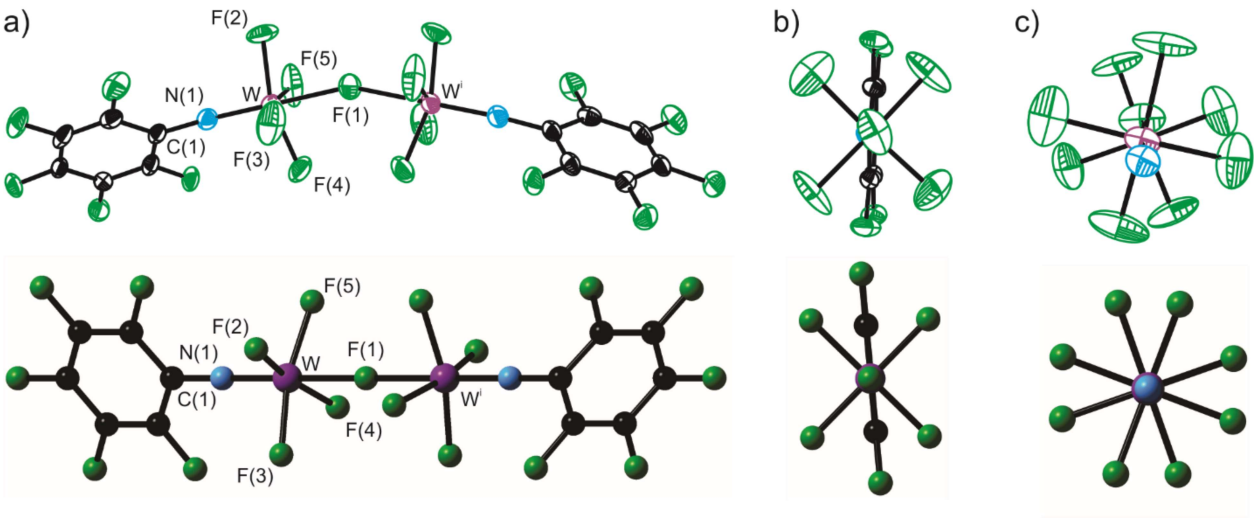

Figure 2. Thermal ellipsoid plot (top) and optimized gas-phase geometry (bottom) of the $W_2(NC_6F_5)_2F_9^-$ anion in $[C_5H_5NH][W_2(NC_6F_5)_2F_9]$: a) side view of the anion; b) end-on view of one $W(NC_6F_5)F_5$ moiety; c) end-on view of the $W_2N_2F_9$ moiety. Thermal ellipsoids are drawn at the 50% probability level.

The W−F_{ax} bond is elongated relative to the W−F_{eq} bonds [2.1010(17) Å vs. 1.854(5)−1.867(6) Å]. It is also longer than the W−F_{ax} bond observed in either salt of the mononuclear anion due to the coordination of the axial fluorido ligand to two tungsten centers and the resultant W−F_{ax} bonds possessing greater ionic character. As a consequence, the W−F_{eq} bonds in the dinuclear anion are shorter than those observed in the mononuclear anion. While the W≡N bond is slightly shorter than that observed in $[N(CH_3)_4][W(NC_6F_5)F_5]$ [1.724(7) vs. 1.755(4) Å], it is not significantly different from that observed in $[C_5H_5NH][W(NC_6F_5)F_5]$ [1.747(2) Å] at 99% confidence. The equatorial fluorido ligands distort from the ideal WF_4 plane towards the axial fluorido ligand [F(1)−W−F: 80.7(2)−81.6(3)°] to a slightly greater extent than in the mononuclear anion, which is expected due to the decreased repulsion by the axial fluorido ligand. As expected, the W−N−C angle is approximately linear [176.3(6)°].

The cation-anion interactions are much weaker in $[C_5H_5NH][W_2(NC_6F_5)_2F_9]$ [N(2)−F = 2.958(11)−3.082(13) Å] than in $[C_5H_5NH][W(NC_6F_5)F_5]$ [N(2)−F(1) = 2.688(2) Å] and have no

significant effect on the W−F_{eq} bond lengths, reflecting a greater degree of weakly coordinating character in the dinuclear anion than in the mononuclear anion.

The predicted D_2-symmetric geometry of the dinuclear anion agrees well with the structure of the anion in the $C_5H_5NH^+$ salt (Figure 2), save for the prediction of a linear W−F_{ax}−W angle, which appears to be highly susceptible to crystal packing effects. Unlike for the $W_2S_2F_9^-$ anion,[18] a bent conformation does not optimize, and the linear geometry is obtained even if the input geometry is bent. Differences in the calculated W−F_{ax}−W angle, however, were not found to significantly influence other geometric properties of the anion.

Vibrational Spectroscopy

Raman spectra were recorded on solid samples of $[C_5H_5NH][W(NC_6F_5)F_5]$, $[N(CH_3)_4][W(NC_6F_5)F_5]$, and $[C_5H_5NH][W_2(NC_6F_5)_2F_9]$ at ambient temperature (Figure 3). Bands corresponding to the $C_5H_5NH^+$ and $N(CH_3)_4^+$ cations were identified based on previous assignments,[28–30] as well as by comparison of the Raman spectra of the $W(NC_6F_5)F_5^-$ salts. Vibrational frequencies were calculated for the $W(NC_6F_5)F_5^-$ and $W_2(NC_6F_5)_2F_9^-$ anions, revealing no imaginary frequencies and excellent agreement with the experimental Raman spectra. As such, assignments of the experimental Raman bands for the $W(NC_6F_5)F_5^-$ and $W_2(NC_6F_5)_2F_9^-$ anions were made on the bases of C_{2v} and D_2 symmetry, respectively. Selected vibrational frequencies (experimental and calculated) for the $W(NC_6F_5)F_5^-$ and $W_2(NC_6F_5)_2F_9^-$ anions are given in Tables 3 and 4, respectively. More complete descriptions of the vibrational frequencies for these anions are given in Tables S4 and S5.

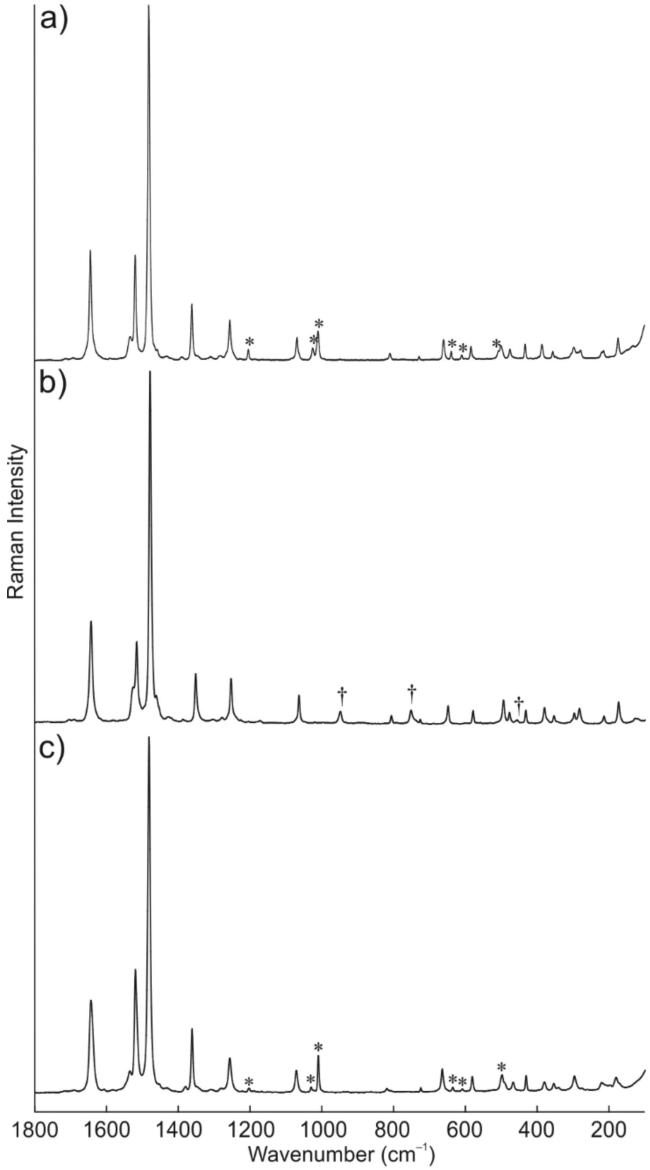

Figure 3. Raman spectra of $W(NC_6F_5)F_5^-$ and $W_2(NC_6F_5)_2F_9^-$ salts: a) $[C_5H_5NH][W(NC_6F_5)F_5]$; b) $[N(CH_3)_4][W(NC_6F_5)F_5]$; c) $[C_5H_5NH][W_2(NC_6F_5)_2F_9]$. Spectra were recorded at ambient temperature in flame-sealed glass m.p. capillaries. Asterisks (*) and daggers (†) denote $C_5H_5NH^+$ and $N(CH_3)_4^+$ cation bands, respectively.

Table 3. Selected Experimental and Calculated Vibrational Frequencies for the $W(NC_6F_5)F_5^-$ Anion

Frequency (cm^{-1})			Assignment (C_{2v})[f,g]
Experimental[a]		Calculated[a,e]	
$C_5H_5NH^+$ Salt[b]	$N(CH_3)_4^+$ Salt[c]		
1482(100)	1481(100)	1521(1055)[976]	A_1, $\nu_s(C_6)$
1362(17)	1353(14)	1358(37)[91]	A_1, $\nu(WN)-\nu(NC)+\nu(C_oF_o)+\nu(C_pF_p)$
1256(12)	1255(12)	1240(38)[117]	A_1, $\nu(WN)-\nu(NC)+\nu(C_mF_m)-(C_pF_p)$
1069(7)	1066(8)	1063(45)[290]	A_1, $\nu(WN)-\nu(C_oF_o)+\nu(C_pF_p)$
810(2)	808(2)	801(13)[<1]	A_1, $\nu(WN)+\nu(NC)-\nu(C_mF_m)$
661(6)	650(5)	647(19)[287]	A_1, $\nu_s(WF_5)$
		607(<1)[269]	B_2, $\nu(WF2)+\nu(WF3)-\nu(WF4)-\nu(WF5)$
		606(<1)[247]	B_1, $\nu(WF2)-\nu(WF3)-\nu(WF4)+\nu(WF5)$
585(4)	581(4)	579(19)[10]	A_1, $\nu(WN)+\delta(C_oC_iC_o)+\delta_s(C_oC_mC_p)$
		575(3)[0]	A_2, $\nu(WF2)-\nu(WF3)+\nu(WF4)-\nu(WF5)$
		548(<1)[165]	A_1, $\nu(WF_{ax})$
501(4)	496(6)	497(35)[8]	A_1, $\nu(WN)-\delta(C_oC_iC_o)-\delta(C_mC_pC_m)$
356(2)	355(2)	353(7)[9]	A_1, $\nu(WN)+\delta_s(C_iC_oF_o)$
298(3)	299(3)	294(6)[41]	A_1, $\delta_s(WF_{eq})$
		282(2)[11]	B_1, $\delta_{ip}(F_{ax}WN)+\delta_{ip}(F2WF5)-\delta_{ip}(F3WF4)$
		280(2)[<0.1]	A_1, $\delta_{ip}(F2WF3)+\delta_{ip}(F4WF5)-\delta_s(C_iC_oF_o)-\delta_s(C_pC_mF_m)$
279(2)	284(4)	279(2)[17]	B_2, $\delta_{op}(F_{ax}WN)+\delta_{ip}(F2WF3)-\delta_{ip}(F4WF5)$
		278(<1)[4]	A_1, $\delta_{ip}(F2WF3)+\delta_{ip}(F4WF5)+\delta_s(C_iC_oF_o)+\delta_s(C_pC_mF_m)$
		201(<0.1)[0]	A_2, $\delta_{op}(F2WF4)-\delta_{op}(F3WF5)$
		187(<1)[10]	B_1, $\delta_{ip}(WNC)+\delta_{ip}(F2WF5)-\delta_{ip}(F3WF4)$
		179(<0.1)[4]	B_2, $\delta_{op}(WNC)+\delta_{ip}(F2WF3)-\delta_{ip}(F4WF5)$
175(6)	175(6)	170(6)[<1]	A_1, $\nu(WN)+\nu(NC)+\delta(C_oC_iC_o)$
		159(<0.1)[4]	B_2, $\delta_{ip}(F2WF3)+\delta_{ip}(F4WF5)$
		115(1)[<0.1]	B_1, $\delta_{ip}(F_{ax}WN)-\delta_{ip}(F2WF5)+\delta_{ip}(F3WF4)$
		93(<0.1)[<0.1]	B_2, $\delta_{op}(F_{ax}WN)-\delta_{ip}(F2WF3)+\delta_{ip}(F4WF5)$
		32(<1)[1]	B_2, $\delta_{op}(WNC)$
		29(<1)[<1]	B_1, $\delta_{ip}(WNC)$
		3(<1)[0]	A_2, $\rho(WF_{eq})-\rho(C_6F_5)$

[a]Normalized Raman intensities are given in parentheses. [b]$C_5H_5NH^+$ bands are observed at 3115(4), 3100(4), 3060(2), 1591(1), 1205(5), 1026(6), 1011(13), 639(4), 610(3), 504(4), and 96(11) cm^{-1}. [c]$N(CH_3)_4^+$ bands are observed at 3044(3), 3033(2), 2999(2), 2970(2), 2934(3), 2831(2), 1176(1), 950(4), 754(5), and 458(2) cm^{-1}. [d]Absolute Raman intensities (in $Å^4\,u^{-1}$) are given in parentheses and absolute IR intensities (in km mol^{-1}) are given in square brackets. [e]Calculated using the B3LYP functional with the Stuttgart basis set augmented by one f-type polarization function (W; $\alpha_f = 0.823$) and *aug*-cc-pVTZ basis set (C, N, F). [f]Symbols and abbreviations denote stretch (ν), bend (δ), rotation (ρ), symmetric (s), antisymmetric (as), in-plane (ip), and out-of-plane (op). [g]Numbering of atoms F2−F5 is consistent with the numbering in Figure 1a.

Table 4. Selected Experimental and Calculated Vibrational Frequencies for the $W_2(NC_6F_5)_2F_9^-$ Anion

Frequency (cm^{-1})		Assignment (D_2)[e,f]
Experimental[a,b]	Calculated[c,d]	
1484(100)	1514(1539)[0]	A, $\nu_s(C_6)$ (s)
1364(18)	1379(167)[0]	A, ν(WN)−ν(NC)+$\nu(C_oF_o)$+$\nu(C_pF_p)$ (s)
1259(9)	1266(126)[0]	A, ν(WN)−ν(NC)+$\nu(C_mF_m)$−(C_pF_p) (s)
1074(6)	1083(104)[0]	A, ν(WN)−$\nu(C_oF_o)$+$\nu(C_pF_p)$ (s)
821(2)	824(31)[0]	A, ν(WN)+ν(NC)−$\nu(C_mF_m)$ (s)
667(7)	665(45)[0]	A, $\nu_s(WF_5)$ (s)
	646(0)[420]	B_3, ν(WF2)+ν(WF3)−ν(WF4)−ν(WF5) (s)
	629(<1)[<1]	B_3, ν(WF2)−ν(WF3)−ν(WF4)+ν(WF5) (s)
	598(3)[0]	A, ν(WF2)−ν(WF3)+ν(WF4)−ν(WF5) (s)
584(5)	582(34)[0]	A, ν(WN)+$\delta(C_oC_iC_o)$+$\delta_s(C_oC_mC_p)$ (s)
501(6)	502(67)[0]	A, ν(WN)−$\delta(C_oC_iC_o)$−$\delta(C_mC_pC_m)$ (s)
	464(<0.1)[576]	B_1, $\nu_{as}(F_{ax}W_2)$
299(6)	296(17)[0]	A, $\delta_s(WF_{eq})$ (s)
	292(<0.1)[13]	B_3, $\delta(F_{ax}WN)$+δ_{ip}(F2WF5)−δ_{ip}(F3WF4)
	292(2)[0]	A, δ_{ip}(F2WF3)+δ_{ip}(F4WF5) (s)
	291(<0.1)[10]	B_2, $\delta(F_{ax}WN)$+δ_{ip}(F2WF5)−δ_{ip}(F3WF4)
	208(<1)[<0.1]	B_2, δ(WNC)+δ_{ip}(F2WF5)−δ_{ip}(F3WF4) (s)
	192(<1)[17]	B_2, δ(WNC)+δ_{ip}(F2WF3)−δ_{ip}(F4WF5) (s)
	186(<0.1)[0]	B_1, δ_{op}(F2WF4)−δ_{op}(F3WF5) (s)
183(5)	181(11)[0]	A, ν(WN)+ν(NC)+$\delta_s(WF_{eq})$+$\delta(C_oC_iC_o)$ (s)
	179(<1)[2]	B_3, $\delta(F_{ax}WN)$+δ_{ip}(F2WF4) (s)
	164(<1)[4]	B_3, $\delta(F_{ax}WN)$−δ_{ip}(F2WF4) (s)
	125(<1)[<0.1]	B_2, $\delta(F_{ax}WN)$ (s)
	112(<1)[<1]	B_3, $\delta(F_{ax}WN)$ (s)
	80(<1)[0]	A, $\nu_s(F_{ax}W_2)$
	40(<1)[1]	B_3, δ(WNC) (s)
	39(<1)[1]	B_2, δ(WNC) (s)
	7(<1)[0]	B_1, $\rho(C_6F_5)$−$\rho(WF_4)$ (s)
	4(<1)[<1]	B_2, $\delta(WF_{ax}W)$
	4(<1)[<1]	B_3, $\delta(WF_{ax}W)$

[a]Normalized Raman intensities are given in parentheses. [b]$C_5H_5NH^+$ bands are observed at 3120(2), 1586(1), 1206(2), 1033(2), 1012(10), 638(2), 611(1), and 494(4), and 98(7) cm^{-1}. [c]Absolute Raman intensities (in $Å^4\,u^{-1}$) are given in parentheses and absolute IR intensities (in km mol^{-1}) are given in square brackets. [d]Calculated using the B3LYP functional with the Stuttgart basis set augmented by one f-type polarization function (W; $\alpha_f = 0.823$) and cc-pVTZ basis set (C, N, F). [e]Symbols and abbreviations denote stretch (ν), bend (δ), rotation (ρ), symmetric (s), antisymmetric (as), axial (ax), equatorial (eq), in-plane (ip), and out-of-plane (op). [f]Mode descriptions are based on the vibration of one $W(NC_6F_5)F_5$ moiety, and the mode is then described as a symmetric (s) or antisymmetric (as) combination of the vibrations of the two moieties. [g]Numbering of atoms F2−F5 is consistent with the numbering in Figure 2a.

The Raman spectra of the $W(NC_6F_5)F_5^-$ salts are highly similar in regards to bands corresponding to the anion, with the majority of observed anion bands being within 2 cm^{-1} of one another and possessing comparable relative intensities (Figure 3). The experimental and predicted Raman frequencies are in excellent agreement with one another. While the 48 vibrational modes are all expected to be Raman-active, the Raman intensities of 16 modes were predicted to be <1 $Å^4\ u^{-1}$, and no obvious experimental counterpart is observed in these cases. The $\nu_s(WF_5)$ mode is found at a higher frequency in the $C_5H_5NH^+$ salt (661 cm^{-1}) than the $N(CH_3)_4^+$ salt (650 cm^{-1}), which is attributed to the hydrogen bond in the $C_5H_5NH^+$ salt decreasing the covalent character the $W{-}F_{ax}$ bond and thereby increasing the covalent character of adjacent bonds. As expected, the predicted frequency for this mode (647 cm^{-1}) agrees more closely with the $N(CH_3)_4^+$ salt. Calculation of the vibrational frequencies reveals extensive coupling of the W≡N stretching vibrations with vibrations of the C_6F_5 group, and as there is no characteristic ν(WN) mode, the nature of the W≡N bond cannot be elucidated easily by consideration of the relative frequencies.

The Raman spectrum of $[C_5H_5NH][W_2(NC_6F_5)_2F_9]$ is highly similar to those of the $W(NC_6F_5)F_5^-$ salts in terms of the frequencies and relative intensities of the anion bands. The experimental and predicted Raman frequencies are in excellent agreement; the decrease from calculated D_2 symmetry to experimentally observed C_2 symmetry likely does not significantly affect mode descriptions, as alteration of the $W{-}F_{ax}{-}W$ angle in the $W_2S_2F_9^-$ anion only affected low-frequency modes corresponding to the fluorine bridge.[18] Due to the weak nature of the fluorine bridge, splittings due to vibrational coupling of the $W(NC_6F_5)F_4$ moieties are typically predicted to be negligible, and cannot be discerned experimentally. Coordination of the axial fluorido ligand to two tungsten centres causes an increase in the covalent character of the adjacent bonds, and the $\nu_s(WF_5)$ mode (667 cm^{-1}) is subsequently higher in frequency than in either $W(NC_6F_5)F_5^-$ salt.

The W≡N stretching vibrations of the dinuclear anion are extensively coupled to vibrations of the C_6F_5 group in manners identical to those observed for the mononuclear anion.

^{19}F NMR Spectroscopy

The nature of the $W(NC_6F_5)F_5^-$ and $W_2(NC_6F_5)_2F_9^-$ anions in solution has been investigated by ^{19}F NMR spectroscopy in CH_3CN at ambient temperature. Spectroscopic data for $[C_5H_5NH][W(NC_6F_5)F_5]$, $[N(CH_3)_4][W(NC_6F_5)F_5]$, and $[C_5H_5NH][W_2(NC_6F_5)_2F_9]$, along with $W(NC_6F_5)F_4{\cdot}NCCH_3$ (observed in a solution of $[C_5H_5NH][W_2(NC_6F_5)_2F_9]$), are given in Table 5.

Table 5. ^{19}F NMR Spectroscopic Parameters for the Fluorido Ligands in the $W(NC_6F_5)F_5^-$ and $W_2(NC_6F_5)_2F_9^-$ Anions and $W(NC_6F_5)F_4{\cdot}NCCH_3$

$\delta(^{19}F)$ (ppm)[a,b]		J (Hz)[a]		
		$^2J(^{19}F-^{19}F)$	$^2J(^{19}F-^{14}N)$	$^1J(^{19}F-^{183}W)$
$[C_5H_5NH][W(NC_6F_5)F_5]$	51.49 (F_{eq}, d)	64.9		42.2
	−61.02 (F_{ax}, m)		37–40	n.o.
$[N(CH_3)_4][W(NC_6F_5)F_5]$	50.93 (F_{eq}, d)	65.1		42.8
	−44.96 (F_{ax}, m)		47.1	68.3
$[C_5H_5NH][W_2(NC_6F_5)_2F_9]$	61.66 (F_{eq}, d)	64.2		41.2
	−110.92 (F_{ax}, n)			n.o.
$W(NC_6F_5)F_4{\cdot}NCCH_3$	61.50 (s)			38.1

[a]Recorded unlocked in CH_3CN at ambient temperature. [b]Abbreviations denote singlet (s), doublet (d), nonet (n), multiplet (m), axial (ax), and equatorial (eq).

In the ^{19}F NMR spectra of $W(NC_6F_5)F_5^-$ salts, the WNF_5 moieties give rise to AX_4 spin systems with ^{183}W satellites (Figure 4a–b). Furthermore, the F_{ax} multiplets – expected to be quintets – are broadened by partially quadrupole-collapsed coupling to ^{14}N at ambient temperature. Resolution enhancement of the spectra allowed for the $^2J(^{19}F_{ax}-^{14}N)$ coupling constants to be ascertained. In the $C_5H_5NH^+$ salt, the outer transitions of the equal-intensity triplets were broadened to the extent that the $^2J(^{19}F_{ax}-^{14}N)$ coupling constant could only be estimated in the range of 37–40 Hz and the ^{183}W satellites could not be observed. However, in the $N(CH_3)_4^+$ salt, splittings due to $^2J(^{19}F_{ax}-^{14}N)$ and $^1J(^{183}W-^{19}F_{ax})$ coupling could be resolved (Figure 5). The

observation of $^{2}J(^{19}F_{ax}–^{14}N)$ coupling corroborates the approximately linear F–W≡N–C skeleton that is observed crystallographically, which results in a small apparent electric-field gradient about the nitrogen atom. Couplings of similar magnitude between the axial fluorido ligand and the nitrogen atom have been observed previously in the $W(NCH_3)F_5^-$ (40 Hz) and $W(NC_2H_5)F_5^-$ (36 Hz) anions.[20,21] Cooling the solutions to −40 °C results in more complete collapse of the $^{2}J(^{19}F_{ax}–^{14}N)$ coupling and the generation of broad quintets (Figure S4). A more detailed discussion of the variable-temperature ^{19}F NMR spectroscopy is provided in the Supporting Information.

In the $N(CH_3)_4^+$ salt, the $^{1}J(^{183}W–^{19}F_{ax})$ coupling constant (68.3 Hz) is higher in magnitude than the $^{1}J(^{183}W–^{19}F_{eq})$ coupling constant (42.2 Hz), despite the more ionic nature of the $W–F_{ax}$ bond. While this phenomenon is counterintuitive based on the relative W–F bond strengths, it has been observed previously for the WSF_5^- anion and is attributed to varying contributions from multiple scalar coupling mechanisms of different signs.[18]

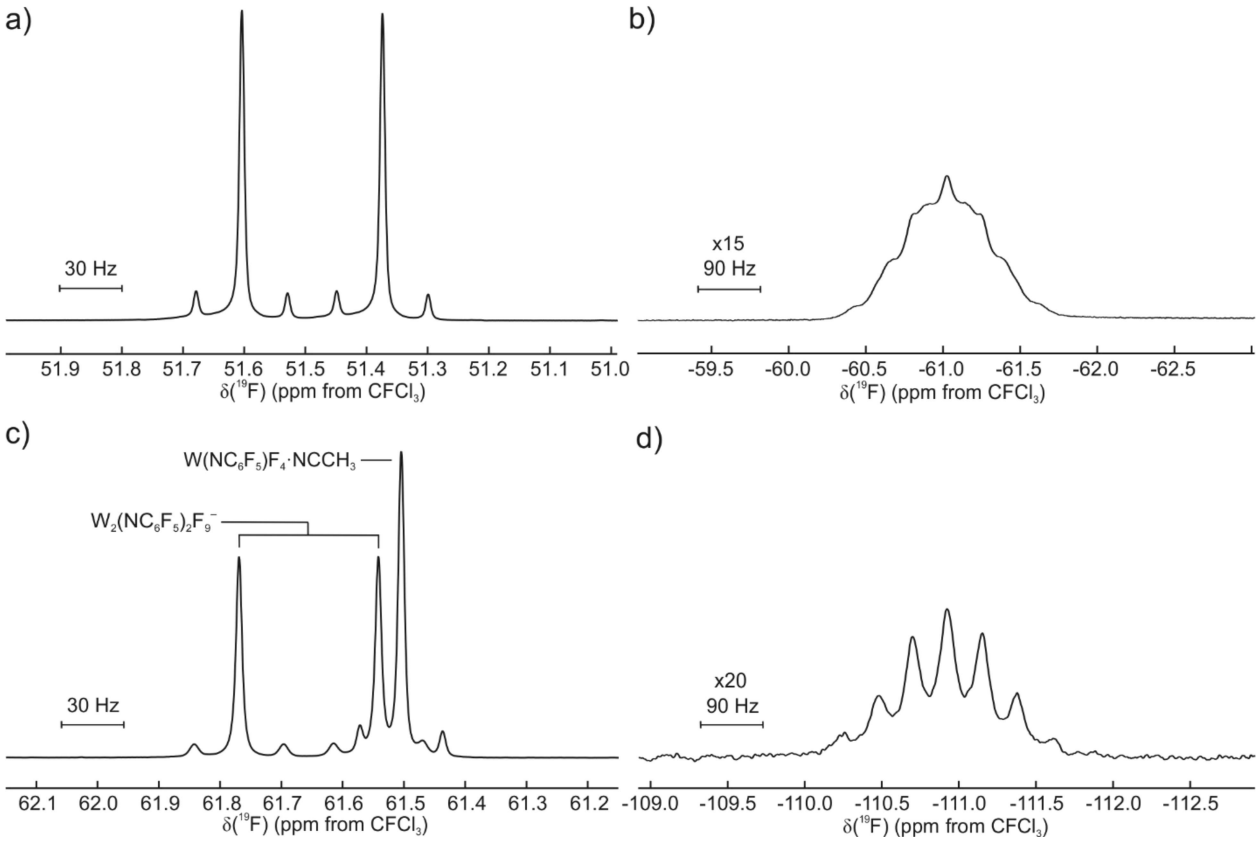

Figure 4. Fluorine-19 NMR spectra of the $W(NC_6F_5)F_5^-$ and $W_2(NC_6F_5)_2F_9^-$ anions: a) F_{eq} doublet in $[C_5H_5NH][W(NC_6F_5)F_5]$; b) F_{ax} multiplet in $[C_5H_5NH][W(NC_6F_5)F_5]$; c) F_{eq} doublet in $[C_5H_5NH][W_2(NC_6F_5)_2F_9]$, including the $W(NC_6F_5)F_4{\cdot}NCCH_3$ impurity; d) F_{ax} nonet in $[C_5H_5NH][W_2(NC_6F_5)_2F_9]$. Spectra were recorded unlocked in CH_3CN at ambient temperature.

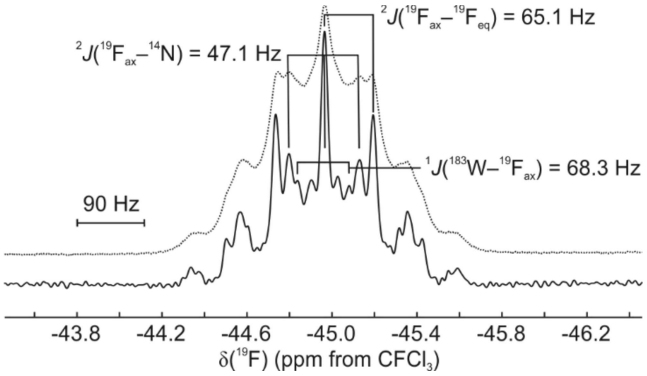

Figure 5. Resolution-enhanced (exponential multiplication = −20 Hz; Gaussian multiplication = 10 Hz; solid trace) and unenhanced (dotted trace) ^{19}F NMR spectra of the F_{ax} multiplet in $[N(CH_3)_4][W(NC_6F_5)F_5]$ in CH_3CN at ambient temperature.

The ^{19}F chemical shifts and coupling constants for the F_{eq} doublet are in excellent agreement with those reported previously for the $C_6F_5NH_3^+$ salt [$\delta(^{19}F_{eq})$ = 52.5 ppm, $^2J(^{19}F_{eq}–^{19}F_{ax})$ = 64.7 Hz, $^1J(^{183}W–^{19}F_{eq})$ = 41.8 Hz].[22] These doublets are much higher in chemical shift than the corresponding F_{ax} multiplets due to a strongly shielding trans influence from the imido ligand. The chemical shift for the F_{ax} multiplet appears lower for the $C_5H_5NH^+$ salt (−61.02 ppm) than the $N(CH_3)_4^+$ salt (−44.96 ppm), suggesting that the hydrogen bond in the $C_5H_5NH^+$ salt persists in solution. The F_{ax} resonance was observed at −63 ppm for the $C_6F_5NH_3^+$ salt,[22] suggesting the presence of a similar hydrogen bond in that salt as well. The F_{eq} and F_{ax} resonances for the $W(NC_6F_5)F_5^-$ anion are found considerably higher in chemical shift than those for the $W(NCH_3)F_5^-$ [$\delta(^{19}F_{eq})$ = 28.0 ppm, $\delta(^{19}F_{ax})$ = −101.5 ppm], $W(NC_2H_5)F_5^-$ [$\delta(^{19}F_{eq})$ = 27.6 ppm, $\delta(^{19}F_{ax})$ = −99.5 ppm], and $W(NC_4H_9)F_5^-$ [$\delta(^{19}F_{eq})$ = 28.7 ppm, $\delta(^{19}F_{ax})$ = −101 ppm] anions.[20,21] This illustrates the electron-withdrawing nature of the C_6F_5 group, which deshields the nuclei and apparently weakens the trans influence of the imido ligand.

In the ^{19}F NMR spectrum of $[C_5H_5NH][W_2(NC_6F_5)_2F_9]$, the $W_2N_2F_9$ moiety gives rise to an AX_8 spin system with ^{183}W satellites being observed for the F_{eq} doublet (Figure 4c–d), in excellent agreement with the ^{19}F NMR spectrum of the $C_6F_5NH_3^+$ salt [$\delta(^{19}F_{eq})$ = 61.9 ppm, $\delta(^{19}F_{ax})$ = −110 ppm, $^2J(^{19}F_{eq}–^{19}F_{ax})$ = 64.7 Hz, $^1J(^{183}W–^{19}F_{eq})$ = 39 Hz].[22] The F_{ax} nonet is broadened to the extent that the outer transitions are not observed, likely due to partially quadrupole-collapsed coupling to the two ^{14}N nuclei (Figure 4d). The $^1J(^{183}W–^{19}F_{ax})$ and/or $^2J(^{19}F_{ax}–^{14}N)$ coupling constants could not be extracted by resolution enhancement or variable-temperature experiments. The fluorido ligands in $W(NC_6F_5)F_4{\cdot}NCCH_3$ – a product of solvolysis of the $W_2(NC_6F_5)_2F_9^-$ anion by CH_3CN – were observed as a singlet with ^{183}W satellites which overlapped partially with the F_{eq} doublet of the dinuclear anion (Figure 4c).

The C_6F_5 groups of these complexes give rise to the expected AA′MM′X spin systems with ^{13}C satellites. The $J(^{19}F-^{19}F)$ coupling constants were ascertained via spectral simulation, and vary only subtly between complexes. The magnitudes and signs of the coupling constants agree well with those observed previously for organic compounds containing C_6F_5N moieties.[31] Further details are provided in the Supporting Information.

Computational Results

Gas-phase geometries were optimized using B3LYP for a series of $W(NR)F_5^-$ anions (R = H, F, CH_3, CF_3, C_6F_5), resulting in stationary points with no imaginary frequencies. The same functional and basis set (*vide infra*) combination was employed in the study of WSF_4,[4] its adducts with nitrogen bases,[4,12] and its derivative anions,[18] and resulted in calculated geometries and vibrational frequencies in good agreement with experimental results. In the case of the $W_2(NC_6F_5)_2F_9^-$ anion, a highly similar basis set was used in which the light atoms were not augmented by diffuse functions. Using these optimized geometries, vibrational frequencies and molecular orbitals (MO) were calculated, and natural-bond-orbital (NBO) analyses were performed, including the calculation of Wiberg bond indices (WBIs).

Optimized Geometries

Selected calculated geometric parameters for the $W(NR)F_5^-$ (R = H, F, CH_3, CF_3, C_6H_5) anions are given in Table 6, and complete geometric parameters are given in Tables S7–S11. The $W(NR)F_5^-$ anions are isostructural (geometrical aspects of the R group notwithstanding) resulting in pseudo-octahedral geometries with linear or near-linear W–N–X (X = H, F, C) angles (Figure S6). Interestingly, in the $W(NCH_3)F_5^-$ anion, the CH_3 group adopts an eclipsed conformation relative to the WF_4 moiety, whereas the CF_3 group is staggered in the $W(NCF_3)F_5^-$ anion (Figure S7). Generally, anions containing fluorinated imido ligands possess shorter W–F bonds, with the

exception being that the W−F_{eq} bonds in the W(NF)F_5^- anion (1.911 Å) are the second longest in the series, behind only those of the W(NCH_3)F_5^- anion (1.914−1.915 Å). There is no obvious division between fluorinated and non-fluorinated imido ligands regarding the W≡N bond length; this bond length is primarily affected by conjugation with the R group (*vide infra*).

Table 6. Selected Calculated Geometric Parameters for the W(NR)F_5^- (R = H, F, CH_3, CF_3, C_6H_5) Anions[a]

	W(NH)F_5^-	W(NF)F_5^-	W(NCH_3)F_5^-	W(NCF_3)F_5^-	W(NC_6H_5)F_5^-
Bond Lengths (Å)					
W−N	1.764	1.763	1.762	1.793	1.783
W−F_{ax}	1.968	1.935	1.969	1.940	1.955
W−F_{eq}	1.909	1.911	1.914−1.915	1.894	1.906
Bond Angles (°)					
W−N−R	180.0	180.0	178.7	179.8	180.00
N−W−F_{ax}	180.0	180.0	179.4	179.9	180.00
F_{ax}−W−F_{eq}	84.2	84.4	84.3−89.3	84.7−84.8	84.8

[a]Calculated using the B3LYP functional with the Stuttgart basis set augmented by one f-type polarization function (W; α_f = 0.823) and *aug*-cc-pVTZ basis set (C, N, F).

Vibrational Frequencies

Selected calculated vibrational frequencies for the W(NR)F_5^- (R = H, F, CH_3, CF_3) anions are given in Table 7, and all vibrational frequencies with complete assignments are given in Tables S12−16**.** The W(NR)F_5^- anions are predicted to exhibit very similar vibrational patterns corresponding to their WNF_5 octahedra; the primary differences manifest in the vibrational coupling between the W≡N stretch and other vibrations. Vibrational coupling is observed in all cases except the W(NH)F_5^- anion, which exhibits a discrete ν(WN) mode at 967 cm^{-1}. However, the nature of the vibrational coupling in the anions is different depending on the R group and cannot be described generally. Thus, differences between the W≡N bond strengths in the W(NR)F_5^- anions cannot be discerned based on their vibrational frequencies. The W(NF)F_5^- anion exhibits antisymmetric and symmetric coupling of the ν(WN) and ν(NF) vibrations at 1371 and

535 cm^{-1}, respectively. The $W(NCH_3)F_5^-$ and $W(NCH_3)F_5^-$ anions exhibit coupling between the ν(WN), ν(NC) and $\delta_s(CX_3)$ (X = H, F) vibrations. Interestingly, the bending vibration couples only with the higher-energy ν(WN)–ν(NC) vibration in the $W(NCH_3)F_5^-$ anion, and only with the lower-energy ν(WN)+ν(NC) vibration in the $W(NCH_3)F_5^-$ anion. In the $W(NC_6H_5)F_5^-$ anion, the ν(WN) vibration exhibits extensive vibrational coupling with various C–C stretches and ring deformations.

The bands at 1347 and 718 cm^{-1} in the Raman spectrum of $[CH_3NH_3][W(NCH_3)F_5]$ had been assigned tentatively as "ν(CNW)";[21] these correspond to the ν(WN)–ν(NC)+$\delta_s(CH_3)$ and ν(WN)+ν(NC) modes in the predicted spectra, respectively. It should be noted that while the calculated frequency for the former mode (1368 cm^{-1}) agrees with the experimental value (1347 cm^{-1}), the latter mode is predicted to be significantly lower in frequency (600 cm^{-1}) than that determined experimentally (718 cm^{-1}).

Table 7. Selected Calculated Vibrational Frequencies for the $W(NR)F_5^-$ (R = H, F, CH_3, CF_3, C_6H_5) Anions

	Frequency (cm^{-1})[a,b]	Assignment[c]
$W(NH)F_5^-$	967(69)[172]	ν(WN)
	639(11)[93]	$\nu_s(WF_5)$
	518(1)[125]	$\nu(WF_{ax})$
$W(NF)F_5^-$	1371(1)[58]	ν(WN)−ν(NF)
	648(24)[64]	$\nu_s(WF_5)$
	552(1)[163]	$\nu(WF_{ax})$
	535(18)[86]	ν(WN)+ν(NF)
$W(NCH_3)F_5^-$	1368(219)[257]	ν(WN)−ν(NC)+$\delta_s(CH_3)$
	634(16)[84]	$\nu_s(WF_5)$
	600(17)[83]	ν(WN)+ν(NC)
	518(1)[132]	$\nu(WF_{ax})$
$W(NCF_3)F_5^-$	1409(108)[1503]	ν(WN)−ν(NC)
	1059(5)[242]	ν(WN)+ν(NC)−$\delta_s(CF_3)$
	712(23)[4]	ν(WN)+ν(NC)+$\delta_s(CF_3)$
	653(12)[200]	$\nu_s(WF_5)$
	548(1)[138]	$\nu(WF_{ax})$
$W(NC_6H_5)F_5^-$	1047(32)[25]	ν(WN)−$\nu_s(C_pC_m)$+$\nu_s(C_iC_o)$
	1025(56)[32]	ν(WN)+$\delta(C_mC_pC_m)$−$\delta(C_oC_iC_o)$
	686(30)[6]	ν(WN)−$\delta(C_mC_pC_m)$−$\delta(C_oC_iC_o)$
	636(8)[273]	$\nu_s(WF_5)$
	533(<1)[169]	$\nu(WF_{ax})$
	231(5)[1]	ν(WN)+ν(NC)+$\delta_s(WF_{eq})$+$\delta(C_oC_iC_o)$

[a]Absolute Raman intensities (in $Å^4\,u^{-1}$) are given in parentheses and absolute IR intensities (in km mol^{-1}) are given in square brackets. [b]Calculated using the B3LYP functional with the Stuttgart basis set augmented by one f-type polarization function (W; $\alpha_f = 0.823$) and *aug*-cc-pVTZ basis set (H, C, N, F). [c]Symbols and abbreviations denote stretch (ν), bend (δ), symmetric (s), axial (ax), and equatorial (eq).

The trend in predicted frequencies of the $\nu(WF_{ax})$ mode correlates inversely with the trend in predicted W−F_{ax} bond lengths. For instance, the $W(NF)F_5^-$ anion has the shortest W−F_{ax} bond (1.935 Å) and the highest frequency $\nu(WF_{ax})$ mode (552 cm^{-1}), and the $W(NCH_3)F_5^-$ anion has the longest bond (1.969 Å) and lowest frequency mode (518 cm^{-1}). Overall, the series of $\nu(WF_{ax})$ frequencies descends in the order $W(NF)F_5^- > W(NCF_3)F_5^- = W(NC_6F_5)F_5^- > W(NC_6H_5)F_5^- > W(NH)F_5^- = W(NCH_3)F_5^-$. The relative frequencies of the $\nu_s(WF_5)$ mode, however, do not correlate with the W−F_{eq} bond lengths, likely because this mode possesses differing proportions of ν(WN), $\nu_s(WF_{eq})$, and $\nu(WF_{ax})$ character depending on the anion.

Molecular Orbitals

The two highest-occupied molecular orbitals in the $W(NR)F_5^-$ anions consist of the $d_{xz/yz}-p_{y/z}$ interactions that comprise the π components of the W≡N bond, along with π* W–F_{eq} and π* N–R interactions. The energies of the MOs containing these interactions, along with the LUMO energies, are given in Table S17. In the $W(NR)F_5^-$ (R = H, F, CH_3, CF_3) anions, the MOs are degenerate or pseudo-generate, whereas in the $W(NC_6H_5)F_5^-$ and $W(NC_6F_5)F_5^-$ anions the MOs are considerably different in energy due to the W≡N π system interacting with the aromatic π system in the HOMO and the sp^2-hybridized σ system of the C_6F_5 group in the HOMO–1 (Figure 6).

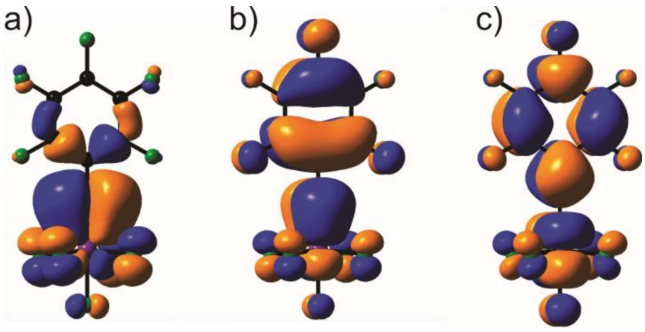

Figure 6. Molecular orbitals in the $W(NC_6F_5)F_5^-$ anion: a) HOMO–1; b) HOMO; c) LUMO. Isosurfaces are drawn at 0.02 e $Å^{-3}$.

The LUMOs of the anions are dominated by π* interactions. In the $W(NR)F_5^-$ (R = H, F, CH_3, CF_3) anions, the LUMO consists of out-of-phase W–F_{eq} interactions, whereas in the $W(NC_6H_5)F_5^-$ and $W(NC_6F_5)F_5^-$ anions, the LUMO consists of out-of-phase W–F_{eq}, W–N and C–C interactions (Figure 6c). The HOMO/LUMO gap is smaller in the $W(NC_6H_5)F_5^-$ and $W(NC_6F_5)F_5^-$ anions than in anions containing non-aromatic R groups as a result of the π* interactions involving the aromatic rings in the HOMO and LUMO. The 428 kJ mol^{-1} HOMO/LUMO gap in the gas-phase $W(NC_6F_5)F_5^-$ anion corresponds to a 280-nm absorption

wavelength, indicating that the difference in energies is slightly overestimated based on the observed yellow colour of the $W(NC_6F_5)F_5^-$ salts.

The HOMO and HOMO−1 of the $W_2(NC_6F_5)_2F_9^-$ anion are pseudo-degenerate and analogous to the HOMO of the $W(NC_6F_5)F_5^-$ anion, whereas the HOMO−4 and HOMO−5 is analogous to the HOMO−1 in the $W(NC_6F_5)F_5^-$ anion. The LUMO is analogous to the LUMO of the $W(NC_6F_5)F_5^-$ anion. The HOMO/HOMO−4 gap is slightly higher in energy than the HOMO/HOMO−1 gap in the $W(NC_6F_5)F_5^-$ anion (123 vs. 97 kJ mol^{-1}), and the HOMO/LUMO gap is predictably similar in energy (437 vs. 428 kJ mol^{-1}).

NBO Analyses

The NBO analyses of the $W(NR)F_5^-$ and $W_2(NC_6F_5)_2F_9^-$ anions reveal the effects of the R group on the electron density at the tungsten center, as well as the W≡N and W−F bonds. Natural-population-analysis charges, WBIs, and total WBIs by atom are given in Tables S18−S24 and summarized in Table S25. Donor-acceptor interaction energies from the NBO second-order perturbation analysis are given in Tables S26−S31. Generally, the WBIs of the W≡N bonds are more than twice those of the $W-F_{eq}$ bonds, corroborating the experimental observation of triple-bond character in imidotungsten(VI) species herein and in previous studies.[23,32] In fact, the WBI of the W≡N bond in the $W(NH)F_5^-$ anion (1.90) is almost exactly triple that of the $W-F_{eq}$ bonds (0.64).

Multiple resonance structures can be drawn to describe the bonding in the W≡N−R moiety of the $W(NR)F_5^-$ anions (Scheme 1). For the parent $W(NH)F_5^-$ anion, resonance structure I clearly predominates and the W≡N bond possesses essentially triple-bond character, inferred from the relative WBIs (vide supra) and the linearity of the W≡N−H moiety. Resonance structure II – the

only structure without formal charges – does not seem to play a significant role for any of the studied anions, as they are all predicted to exhibit linear (or near-linear) W≡N–R moieties.

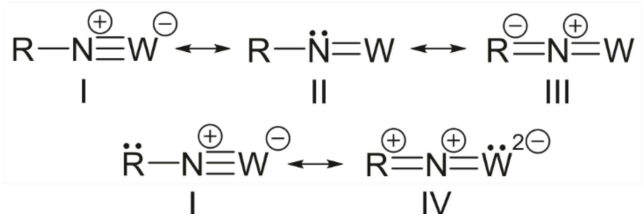

Scheme 1. Resonance structures contributing to bonding in the W≡N–R moiety of the $W(NR)F_5^-$ (R = H, F, CH_3, CF_3, C_6H_5, C_6F_5) and $W_2(NC_6F_5)_2F_9^-$ anions.

In the $W(NR)F_5^-$ anions (R = F, CF_3, C_6H_5, C_6F_5), conjugation is observed, resulting in a decrease in the WBIs of the W≡N bond (1.59–1.81) relative to the $W(NH)F_5^-$ anion. Conjugation between the W≡N bond and R group can manifest due to π-electron withdrawal (resonance structure III) or donation (resonance structure IV) by the R group, which weakens the W≡N bond in both cases. The WBIs of the W≡N bonds and predicted W≡N bond lengths are, as expected, inversely correlated. However, this trend is clearer in the anions with the highest degree of resonance (R = CF_3, C_6H_5, C_6F_5); the W≡N bond lengths of the remaining $W(NR)F_5^-$ anions (R = H, F, CH_3) are practically indistinguishable (1.762–1.764 Å).

In the $W(NCF_3)F_5$ and $W(NC_6F_5)F_5^-$ anions, the π-electron-accepting nature of the CF_3 and C_6F_5 groups favors the invocation of resonance structure III as contributing to the decrease in the W≡N bond order. This is corroborated by the higher positive charges on tungsten in these anions (+2.45 to +2.47) than in the $W(NH)F_5^-$ anion (+2.39) and the NBO second-order perturbation analyses, which reveal substantial energies for interactions between the W≡N bonds and the π-electron-accepting groups (CF_3: 203 kJ mol^{-1}, C_6F_5: 178 kJ mol^{-1}). The converse is true for the $W(NF)F_5^-$ anion, which contains the mildly π-electron-donating nitrogen-bound fluorine

atom. An interaction energy of 110 kJ mol^{-1} is calculated for π-electron donation from the fluorine atom to the W≡N bond, resulting in a slight decrease in W≡N bond order and lowering of the positive charge on tungsten (+2.31), consistent with a contribution from resonance structure IV. The C_6H_5 group may act as a π-electron donor and acceptor, and the NBO second-order perturbation analysis returns a slightly larger interaction energy for π-electron withdrawal (138 kJ mol^{-1}) versus donation (103 kJ mol^{-1}). As such, resonance structures III and IV likely contribute to the nature of the W≡N−R moiety of the $W(NC_6H_5)F_5^-$ anion, explaining why the charge on tungsten (+2.41) is very close to that in the $W(NH)F_5^-$ anion.

In the $W_2(NC_6F_5)_2F_9^-$ anion, the WBI of the W−F_{ax} bond (0.27) is approximately half that predicted for the $W(NC_6F_5)F_5^-$ anion (0.53), consistent with the change from a terminal to bridging coordination environment decreasing the covalent character of the W−F_{ax} bonds. The positive charge on the tungsten centres (+2.36) is lower than in the $W(NC_6F_5)F_5^-$ anion despite the decreased covalent character of the W−F_{ax} bonds, which is seemingly due to overcompensatory donation from the imido ligand; the WBI of the W≡N bond (1.76) is much higher than in the $W(NC_6F_5)F_5^-$ anion (1.59).

Conclusions

Convenient routes to $W(NC_6F_5)F_5^-$ and $W_2(NC_6F_5)_2F_9^-$ salts have been reported, which have been fully characterized in the solid state and in solution. The structural properties of these anions are somewhat dependent on the cation. Cation-anion interactions in the $C_5H_5NH^+$ salt affect structure and bonding in the anion, which is observed crystallographically and spectroscopically in the solid state and in solution. Meanwhile, the $W_2(NC_6F_5)_2F_9^-$ anion is highly susceptible to conformational distortions in the solid state, as inferred from the variations between the crystal structures of the $C_5H_5NH^+$ and previously reported $C_6F_5NH_3^+$ salts.[22] The Raman spectra of

$W(NC_6F_5)F_5^-$ and $W_2(NC_6F_5)_2F_9^-$ salts reveal extensive coupling of the W≡N stretching vibration with symmetric vibrations of the C_6F_5 group, and these bands have been assigned unambiguously with the aid of DFT calculations.

To complement the experimental studies, a suite of $W(NR)F_5^-$ anions has been studied by DFT (B3LYP) methods. The calculations reveal that the R group can have substantial effects on the structural and electronic properties of the anion. The calculated W–F_{ax} bond lengths suggest that the tungsten center is more electrophilic in anions containing fluorinated R groups than in their hydrogen-containing analogs. The calculated W≡N bond lengths, MOs, as well as the NBO analyses, further validate the designation of a triple bond between tungsten and nitrogen, although conjugation between the W≡N bond and the R group can considerably decrease the W≡N bond order.

Experimental

Materials and Apparatuses

Caution: Anhydrous HF can cause severe burns upon contact or inhalation; appropriate safety measures should be implemented during handling. Tungsten hexafluoride and its derivatives synthesized herein produce HF upon contact with even trace amounts of moisture and should be manipulated only under rigorously dry conditions.

All reactions were carried out in heat-sealed ¼”-o.d. FEP reactors which were connected to either stainless-steel or Kel-F valves via flared fittings. Volatile materials were distilled on a Pyrex vacuum line equipped with glass valves fitted with 6-mm-o.d. PTFE J. Young stopcocks, with the exceptions of WF_6, which was distilled through a nickel/316 stainless-steel vacuum line equipped with 316 stainless-steel valves (Autoclave Engineers) and pre-passivated with 100% F_2, and anhydrous HF, which was distilled through a FEP manifold connected to and pre-passivated

on the aforementioned metal vacuum line. Solid materials were handled in a dry box (Omni Lab, Vacuum Atmospheres) under an atmosphere of dry N_2.

Dichloromethane was distilled from a solvent system onto 4-Å molecular sieves and then distilled onto fresh sieves. Acetonitrile (Baker, 99.8%) was dried over P_4O_{10} and doubly distilled onto 3-Å molecular sieves. Sulfur dioxide (Matheson) was dried over CaH_2. Tungsten hexafluoride (Ozark-Mahoning) and $C_6F_5NH_2$ (Sigma-Aldrich, 99%) were used as provided. Anhydrous hydrogen fluoride (Air Products, 99.9%) was dried with 100% F_2 and distilled onto $K_2[NiF_6]$. The $WF_6{\cdot}NC_5H_5$ adduct and $[(CH_3)_4N][WF_7]$ were prepared as described previously.[33,34]

Syntheses

$[C_5H_5NH][W(NC_6F_5)F_5]$

In the dry box, $WF_6{\cdot}NC_5H_5$ (0.568 g, 1.51 mmol) and $C_6F_5NH_2$ (0.291 g, 1.59 mmol) were added to a ¼”-o.d. FEP reactor at ambient temperature, causing immediate formation of an orange substance upon contact of the solids; the reactor was kept at −80 °C to curtail further solid-state reactions. Dichloromethane (1.097 g) was distilled into the reactor at −196 °C and warmed to ambient temperature, resulting in the formation of an orange solution. Volatile materials were removed under dynamic vacuum at ambient temperature (with constant agitation) for 1 h, and at 45 °C over 30 min, yielding $[C_5H_5NH][W(NC_6F_5)F_5]$ (0.809 g, 1.50 mmol, 99.4% yield w.r.t. $WF_6{\cdot}NC_5H_5$) as a coarse yellow powder. An impurity of WOF_5^- (1 mol%) was observed by ^{19}F NMR spectroscopy. $\delta(^1H)$ (ppm, CH_3CN, unlocked): $C_5H_5NH^+$, 13.78 (s, H_N), 8.73 (d, H_o, $^3J(^1H_o{-}^1H_m)$ = ~6 Hz), 8.60 (t, H_p, $^3J(^1H_m{-}^1H_p)$ = ~8 Hz), 8.05 (t, H_m).

$[N(CH_3)_4][W(NC_6F_5)F_5]$

In the dry box, $[N(CH_3)_4][WF_7]$ (0.2324 g, 0.594 mmol) and $C_6F_5NH_2$ (0.1150 g, 0.628 mmol) were added to a ¼”-o.d. FEP reactor. Acetonitrile (0.300 g) was distilled into the reactor at

−196 °C and warmed to ambient temperature, resulting in the formation of an orange solution. Volatile materials were removed under dynamic vacuum at ambient temperature (with constant agitation) for 30 min, and at 45 °C for 30 min, yielding $[N(CH_3)_4][W(NC_6F_5)F_5]$ (0.317 g, 0.594 mmol, 100% yield w.r.t $[N(CH_3)_4][WF_7]$) as a coarse yellow powder. Impurities of WOF_5^- (1 mol%), $C_6F_5NH_2$ (2 mol%), $W_2(NC_6F_5)_2F_9^-$ (trace), and HF (trace) were observed by ^{19}F NMR spectroscopy. $\delta(^1H)$ (ppm, CH_3CN, unlocked): $(CH_3)_4N^+$, 3.07 (s, CH_3).

$[C_5H_5NH][W_2(NC_6F_5)_2F_9]$

In the dry box, $[C_5H_5NH][W(NC_6F_5)F_5]$ (0.383 g, 0.709 mmol) was added to the straight arm of a T-shaped ¼"-o.d. FEP reactor. Anhydrous HF (0.136 g, 6.80 mmol) was distilled into the reactor at −196 °C and warmed to ambient temperature, resulting in the formation of a deep red solution. Cooling the solution to −25 °C resulted in the precipitation of yellow crystals; the solution was then decanted from these crystals into the side arm of the reactor, and the HF was partially condensed back into the straight arm at −196 °C. This was repeated five times, resulting in yellow crystals remaining in the straight arm, and a red solution in the side arm. Volatile materials were removed under dynamic vacuum at −70 °C for 2 h and at ambient temperature over 30 min, yielding $[C_5H_5NH][W_2(NC_6F_5)_2F_9]$ (0.266 g, 0.271 mmol, 76.5% yield w.r.t $[C_5H_5NH][W(NC_6F_5)F_5]$) in the straight arm as a yellow powder. Impurities of $W(NC_6F_5)F_5^-$ (3−5 mol%), $W_2(NC_6F_5)OF_9^-$ (2 mol%), $C_6F_5NH_2$ (1−2 mol%), and HF (trace) were observed by ^{19}F NMR spectroscopy (the impurity of $W(NC_6F_5)F_5^-$ is in addition to that generated by solvolysis of the product in CH_3CN). $\delta(^1H)$ (ppm, CH_3CN, unlocked): $C_5H_5NH^+$, 13.18 (tt, H_N, $^1J(^{14}N-^1H_N)$ = 68.4 Hz), 8.71 (t, H_o, $^3J(^1H_N-^1H_o) = {}^3J(^1H_o-^1H_m)$ = ~6 Hz), 8.61 (tt, H_p, $^3J(^1H_m-^1H_p)$ = ~8 Hz, $^5J(^1H_N-^1H_p)$ = ~1 Hz), 8.05 (t, H_m).

The side arm contained a yellow-orange powder than consisted of $[C_5H_5NH][W(NC_6F_5)F_5]$ and $[C_5H_5NH][F(HF)_n]$ as determined by Raman spectroscopy.

X-ray Crystallography

Crystal Growth and Mounting

Long, yellow plates of $[C_5H_5NH][W(NC_6F_5)F_5]$ were grown in a ¼"-o.d. FEP reactor by cooling a CH_2Cl_2 solution to −35 °C, followed by slow removal of the solvent at that temperature. Yellow blocks of $[(CH_3)_4N][W(NC_6F_5)F_5]$ and thin yellow plates of $[C_5H_5NH][W_2(NC_6F_5)_2F_9]$ were grown in ¼"-o.d. FEP reactors from CH_3CN solutions by slow removal of the solvent at −40 °C. The reactors were cut on an aluminum trough cooled to −80 °C by a stream of dry N_2 and the crystals were deposited onto the trough. The selected crystals were affixed to a Nylon cryo-loop submerged in perfluorinated polyether oil (Fomblin Z-25) and transferred to the goniometer using liquid-N_2-cooled cryo-tongs.

Data Collection and Reduction

The crystals were centered on a Rigaku SuperNova diffractometer equipped with a Dectris Pilatus 3R 200K-A hybrid-pixel-array detector, a four-circle κ goniometer, and sealed, graphite-monochromated MoK_α and CuK_α X-ray sources. Data was collected using the MoK_α source (λ = 0.71073 Å) at 100 K. Crystals were screened for quality before a pre-experiment was run to determine the unit cell, and a data collection strategy was calculated based on the determined unit cell and the quality of the preliminary data. This strategy was optimized to collect five-fold redundant data at a resolution of 0.77 Å. The data was processed using CrysAlisPro,[35] which applied necessary Lorentz and polarization corrections to the integrated data and scaled the data. A numerical (Gaussian-grid) absorption correction was generated based upon the indexed faces of

the crystal. Upon reduction of the data, frames with a $R_{int} > 0.2$ were omitted, which did not adversely affect the completeness of the data.

Structure Solution and Refinement

Atom positions were determined using the intrinsic phasing method (ShelXT)[36] and were refined using least-squares refinement (ShelXL).[37] Non-hydrogen atoms were refined anisotropically and recommended weights for the atoms were determined before hydrogen atoms were introduced using a riding model (HFIX). In the case of $[C_5H_5NH][W(NC_6F_5)F_5]$, the nitrogen-bound hydrogen atom could be located in the Fourier difference map, and as such its position was freely refined. The maximum and minimum electron density in the Fourier difference map were located near the tungsten atoms in all cases. Structure solution and refinement were performed with the aid of Olex2.[38]

Crystallographic data have been deposited with the Cambridge Crystallographic Data Centre as CCDC 1566648 ($[C_5H_5NH][W(NC_6F_5)F_5]$), 1566649 ($[N(CH_3)_4][W(NC_6F_5)F_5]$), and 1566650 ($[C_5H_5NH][W_2(NC_6F_5)_2F_9]$. Copies of the data can be obtained free of charge from CCDC via http://www.ccdc.cam.ac.uk.

Raman Spectroscopy

All Raman spectra were recorded on powdered samples in flame-sealed m.p. capillaries using a Bruker RFS-100 Raman spectrometer outfitted with a quartz beam-splitter and liquid-N_2-cooled germanium detector. The 1064-nm line of a Nd:YAG laser was used for excitation of the sample, and back-scattered (180°) radiation was sampled. The usable Stokes range of the collected data was 85 to 3500 cm^{-1} with a resolution of 2 cm^{-1}. The laser power was typically set to 150 mW.

NMR Spectroscopy

All NMR spectra were recorded in heat-sealed 4-mm o.d. FEP tubes in 5-mm o.d. glass inserts using a Bruker Avance II 300 MHz spectrometer equipped with a 5-mm broadband probe. Spectra were recorded unlocked in dilute CH_3CN solutions, and referenced externally to $CFCl_3$ (^{19}F) and $Si(CH_3)_4$ (^1H) at 20 °C. Spectral simulations were performed using Mestre Nova.[39]

Computational Details

All DFT calculations were performed using the B3LYP functional. The Stuttgart basis set augmented by one f-type polarization function ($\alpha_f = 0.823$),[40] and the associated pseudopotentials, were used for tungsten. For the $W(NR)F_5^-$ anions, the *aug*-cc-pVTZ basis set was used for hydrogen, carbon, nitrogen, and fluorine, whereas for the $W_2(NC_6F_5)_2F_9^-$ anion, the cc-pVTZ basis set was used. Geometry optimizations were performed using analytic gradient methods, and the vibrational-frequency and MO calculations, as well as the NBO analyses, were performed using the geometries optimized at the same level of theory. Calculations were performed using Gaussian 09 (revision D.01),[41] and NBO (version 6.0) was used for the NBO analyses.[42] The GaussView program was used to visualize the vibrational displacements that form the basis for the vibrational mode descriptions.[43]

Supporting Information

Crystallographic data collection and refinement parameters (Table S1); experimental and calculated geometric parameters for the $W(NC_6F_5)F_5^-$ and $W_2(NC_6F_5)_2F_9^-$ anions (Tables S2–S3); crystal packing diagrams (Figures S1–S3); experimental and calculated vibrational frequencies for the $W(NC_6F_5)F_5^-$ and $W_2(NC_6F_5)_2F_9^-$ anions (Tables S4–S5); variable-temperature ^{19}F NMR spectra (Figure S4); ^{19}F NMR spectral simulations (Table S6 and Figure S5); calculated geometric parameters for the $W(NR)F_5^-$ (R = H, F, CH_3, CF_3, C_6H_5) anions (Tables S7–S11); optimized gas-

phase geometries of the $W(NR)F_5^-$ (R = H, F, CH_3, CF_3, C_6H_5, C_6F_5) and $W_2(NC_6F_5)_2F_9^-$ anions (Figure S6−S7); calculated vibrational frequencies for the $W(NR)F_5^-$ (R = H, F, CH_3, CF_3, C_6H_5) anions (Tables S12−S16); selected MO energies (Table S17); NPA charges, total WBIs by atom, and WBIs for the $W(NR)F_5^-$ (R = H, F, CH_3, CF_3, C_6H_5, C_6F_5) and $W_2(NC_6F_5)_2F_9^-$ anions (Tables S18−S25); energies of donor-acceptor interactions from the NBO second-order perturbation analyses for the $W(NR)F_5^-$ (R = H, F, CH_3, CF_3, C_6H_5, C_6F_5) and $W_2(NC_6F_5)_2F_9^-$ anions (Tables S26−S31).

Acknowledgements

We would like to thank the Natural Sciences and Engineering Research Council of Canada (M.G. and S.D.W.: Discovery grants; D.T.: CGS-M scholarship) and the University of Lethbridge for supporting this work. We would also like to thank the university for awarding the SGS Dean's Scholarship and Tuition Award to D.T. Computational studies were performed using equipment funded through the Canada Foundation of Innovation, as well as resources made available through Westgrid and Compute/Calcul Canada.

References

(1) Ruff, O. Über die Darstellung und Eigenschaften von Fluoriden des sechswertigen Wolframs. *Z. Anorg. Chem.* **1907**, *52* (1), 256–269.

(2) Edwards, A. J.; Jones, G. R. Fluoride Crystal Structures. Part I. Tungsten Oxide Tetrafluoride. *J. Chem. Soc.* **1968**, 2074.

(3) Holloway, J. H.; Kaučič, V.; Russell, D. R. Synthesis, Chemistry, and Crystal Structures of High-Valent Transition-Metal Chalcogenide Fluorides and Their Derivatives. *J. Chem. Soc., Chem. Commun.* **1983**, *0* (19), 1079–1081.

(4) Nieboer, J.; Hillary, W.; Yu, X.; Mercier, H. P. A.; Gerken, M. Syntheses,

Characterization, and Computational Study of WSF_4 and $WSF_4 \cdot CH_3CN$. *Inorg. Chem.* **2009**, *48* (23), 11251–11258.

(5) Tucker, P. A.; Taylor, P. A.; Holloway, J. H.; Russell, D. R.; IUCr. The Adduct XeF_2 .WOF_4. *Acta Crystallogr. Sect. B Struct. Crystallogr. Cryst. Chem.* **1975**, *31* (3), 906–908.

(6) Arnaudet, L.; Bougon, R.; Ban, B.; Charpin, P.; Isabey, J.; Lance, M.; Nierlich, M.; Vigner, J. Preparation, Characterization, and Crystal Structure of the Adducts $WOF_4.nC_5H_5N$ (n = 1, 2). *Inorg. Chem.* **1989**, *28* (2), 257–262.

(7) Arnaudet, L.; Bougon, R.; Ban, B.; Charpin, P.; Isabey, J.; Lance, M.; Nierlich, M.; Vigner, J. 2,2'-Bipyridyl Adducts of Tungsten Oxide Fluorides: Preparation and Characterization of WOF_4 Bipy and WO_2F_2 Bipy; Crystal Structure of WO_2F_2 Bipy. *Can. J. Chem.* **1990**, *68* (3), 507–512.

(8) Arnaudet, L.; Bougon, R.; Ban, B.; Lance, M.; Kaska, W. C. Adducts of Tungsten Oxide Tetrafluoride with 1,8 - Naphthyridine and 2,7-Dimethyl - 1,8- Naphthyridine : Preparation and Characterization of WOF_4.napy and WOF_4.dmnapy. *J. Fluorine Chem.* **1991**, *53* (2), 171–180.

(9) Arnaudet, L.; Bougon, R.; Ban, B.; Lance, M.; Nierlich, M.; Vigner, J. Preparation, Characterization, and Crystal Structure of the Tungsten Hexafluoride and Tetrafluoride Oxide Adducts WF_6.F-Py and WOF_4.F-Py (F-Py = 2-Fluoropyridine). *Inorg. Chem.* **1993**, *32* (7), 1142–1146.

(10) Levason, W.; Reid, G.; Zhang, W. Coordination Complexes of the tungsten(VI) Oxide Fluorides WOF_4 and WO_2F_2 with Neutral Oxygen- and Nitrogen-Donor Ligands. *J. Fluorine Chem.* **2016**, *184*, 50–57.

(11) Emsley, J. W.; Levason, W.; Reid, G.; Zhang, W.; De Luca, G. Phosphine and

Diphosphine Complexes of tungsten(VI) Oxide Tetrafluoride. *J. Fluorine Chem.* **2017**, *197*, 74–79.

(12) Nieboer, J.; Yu, X.; Chaudhary, P.; Mercier, H. P. A.; Gerken, M. Synthesis, Characterization, and Computational Study of $WSF_4 \cdot NC_5H_5$. *Z. Anorg. Allg. Chem.* **2012**, *638* (3–4), 520–525.

(13) Bougon, R.; Bui Huy, T.; Charpin, P. Acid Properties of the Oxytetrafluorides of Molybdenum, Tungsten, and Uranium toward Some Inorganic Fluoride Ion Donors. *Inorg. Chem.* **1975**, *14* (8), 1822–1830.

(14) Wilson, W. W.; Christe, K. O. Perfluoroammonium and Cesium Fluorotungstates. *Inorg. Chem.* **1981**, *20* (12), 4139–4143.

(15) Katayama, Y.; Hagiwara, R.; Ito, Y. Acid-Base Reactions of Tungsten and Uranium Oxide Fluorides in Anhydrous Hydrogen Fluoride. *J. Fluorine Chem.* **1995**, *74* (1), 89–95.

(16) Atherton, M. J.; Holloway, J. H. Transition-Metal Thiofluorides; Preparation of WSF_4 and Related Anions. *J. Chem. Soc., Chem. Commun.* **1977**, 424.

(17) Hilbers, M.; Läge, M.; Mattes, R. Preparation and Structure of $(Ph_3P)_2N[WSF_5]$. *Inorg. Chim. Acta* **1992**, *201* (1), 1–3.

(18) Nieboer, J.; Haiges, R.; Hillary, W.; Yu, X.; Richardet, T.; Mercier, H. P. A.; Gerken, M. Fluoride-Ion Acceptor Properties of WSF_4: Synthesis, Charcaterization, and Computational Study of the WSF_5^- and $W_2S_2F_9^-$ Anions and ^{19}F NMR Spectroscopic Characterization of the $W_2OSF_9^-$ Anion. *Inorg. Chem.* **2012**, *51* (11), 6350–6359.

(19) Kokunov, Y. V.; Chubar, Y. D.; Bochkareva, V. A.; Buslaev, Y. A. Oxolysis, Thiolysis, and Iminolysis of Tungsten Hexafluoride. *Koord. Khim.* **1975**, *1* (8), 1100–1105.

(20) Chambers, O. R.; Rycroft, D. S.; Sharp, D. W. A.; Winfield, J. M. Aminolysis Reactions

of Tungsten Hexafluoride: N-alkylimidofluorotungstates(VI). *Inorg. Nucl. Chem. Lett.* **1976**, *12* (7), 559–561.

(21) Chambers, O. R.; Harman, M.; Rycroft, D. S.; Sharp, D. W. A.; Winfield, J. M. Alkylimidotungsten(VI) Fluorides. *J. Chem. Res. (M)* **1977**, 1849–1876.

(22) Fawcett, J.; Griffith, G. A.; Peacock, R. D.; Russell, D. R. The Reaction between Tungsten Hexafluoride and Pentafluoroaniline. *Polyhedron* **1988**, *7* (19), 2015–2022.

(23) Görge, A.; Dehnicke, K.; Fenske, D. Synthesis and Crystal Structure of [Na-15-Crown-5][WF_5(NCl)]. *Z. Naturforsch. B* **1989**, *44* (2), 117–120.

(24) Stenger, H.; Dehnicke, K.; Hiller, W. [K(18-Crown-6)][WF_5(NCl)]; Synthesis and Crystal Structure. *Z. Naturforsch. B* **1992**, *47* (7), 1054–1056.

(25) Dietrich, A.; Neumüller, B.; Dehnicke, K. Die Kristallstruktur von K[F_5W(≡NCl)]. *Z. Anorg. Allg. Chem.* **2000**, *626* (12), 2443–2445.

(26) Rhiel, M.; Wocadlo, S.; Massa, W.; Dehnicke, K. Reaktionen von $MoNCl_3$ Und $WNCl_3$ mit elementarem Fluor. Kristallstrukturen von [$MoO_2F_2(THF)_2$] und [WF_4(NCl)(CH_3CN)]. *Z. Anorg. Allg. Chem.* **1996**, *622* (7), 1195–1199.

(27) Fenske, D.; Kujanek, R.; Dehnicke, K. CPh_3^+[Ph_3CNWCl_4(μ-F)$WNCl_2$(μ-F)Cl_4WNCPh_3]$^-$; Synthese und Kristallstruktur eines dreikernigen Nitrido-Nitren-Komplexes des Wolframs. *Z. Anorg. Allg. Chem.* **1983**, *507* (12), 51–58.

(28) Cook, D. Vibrational Spectra of Pyridinium Salts. *Can. J. Chem.* **1961**, *39* (10), 2009–2024.

(29) Foglizzo, R.; Novak, A. Low-Frequency Infrared and Raman Spectra of Hydrogen-Bonded Pyridinium Halides. *J. Chem. Phys.* **1969**, *50* (12), 5366–5373.

(30) Kabisch, G. Raman Spectra and Crystal Structure of Polycrystalline

Tetramethylammonium Salts. *J. Raman Spectrosc.* **1980**, *9* (5), 279–285.

(31) Hogben, M. G.; Graham, W. A. G. Chemical Shifts and Coupling Constants in Pentafluorophenyl Derivatives. I. Correlations of Chemical Shifts, Coupling Constants, and .pi.-Electronic Interactions. *J. Am. Chem. Soc.* **1969**, *91* (2), 283–291.

(32) Harman, M.; Sharp, D. W. A.; Winfield, J. M. ^{1}H-^{14}N Spin-Spin Coupling in methylimidotungsten(VI) Tetrafluoride, Acetonitrile. *Inorg. Nucl. Chem. Lett.* **1974**, *10* (2), 183–185.

(33) Arnaudet, L.; Bougon, R.; Buu, B.; Lance, M.; Nierlich, M.; Thuéry, P.; Vigner, J. Characterization of the Adducts $WF_6 \cdot py$ and $WF_6 \cdot 2py$ (Py = Pyridine): Crystal Structure of $WF_6 \cdot 2py$. *J. Fluorine Chem.* **1995**, *71* (1), 123–129.

(34) Giese, S.; Seppelt, K. Structural Principles in Seven-Coordinate Subgroup Compounds: The Complex Anions MoF_7^-, WF_7^-, and $ReOF_6^-$. *Angew. Chem. Int. Ed. Engl.* **1994**, *33* (4), 461–463.

(35) CrysAlisPro. Agilent Technologies, Ltd.: Yarnton, Oxfordshire, England **2014**.

(36) Sheldrick, G. M. SHELXT. University of Göttingen, Germany, **2015**.

(37) Sheldrick, G. M. SHELXL. University of Göttingen, Germany, **2015**.

(38) Dolomanov, O. V.; Bourhis, L. J.; Gildea, R. J.; Howard, J. A. K.; Puschmann, H. Olex2, version 1.2. OlexSys Ltd.: Durham University, UK, **2017**.

(39) MestRe Nova, version 9.0. Mestrelab Research S.L.: Santiago de Compostela, Spain, **2014.**

(40) Ehlers, A. W.; Böhme, M.; Dapprich, S.; Gobbi, A.; Höllwarth, A.; Jonas, V.; Köhler, K. F.; Stegmann, R.; Veldkamp, A.; Frenking, G. A Set of F-Polarization Functions for Pseudo-Potential Basis Sets of the Transition Metals Sc-Cu, Y-Ag and La-Au. *Chem.*

Phys. Lett. **1993**, *208* (1–2), 111–114.

(41) Frisch, M. J.; Trucks, G. W.; Schlegel, H. B.; Scuseria, G. E.; Robb, M. A.; Cheeseman, J. R.; Scalmani, G.; Barone, V.; Petersson, G. A.; Nakatsuji, H.; et al. Gaussian 09, Revision D.01. Gaussian, Inc.: Wallingford, CT, 2016.

(42) Glendening, E. D.; Badenhoop, J. K.; Reed, A. E.; Carpenter, J. E.; Bohmann, J. A.; Morales, C. M.; Landis, C. R.; Weinhold, F. NBO 6.0. Theoretical Chemistry Institute, University of Wisconsin: Madison, WI, 2013.

(43) GaussView, version 5.0. Gaussian, Inc.: Wallingford, CT, **2016.**

Table of Contents Sypnosis and Graphic

Facile syntheses of $W(NC_6F_5)F_5^-$ and $W_2(NC_6F_5)_2F_9^-$ salts have been developed. These salts have been fully characterized in the solid state by X-ray crystallography and Raman spectroscopy, and in solution by ^{19}F and ^{1}H NMR spectroscopy. In addition, complementary DFT studies (B3LYP) have been conducted on the $W(NR)F_5^-$ (R = H, F, CH_3, CF_3, C_6H_5, C_6F_5) and $W_2(NC_6F_5)_2F_9^-$ anions in order to relate their structural and electronic properties.

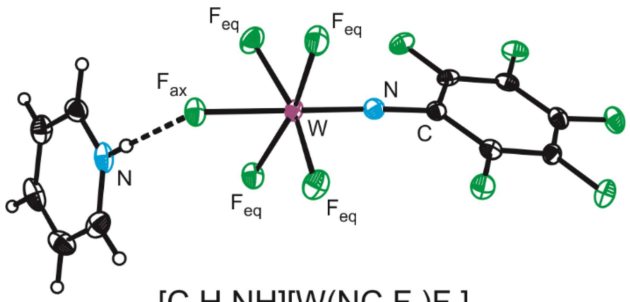

$[C_5H_5NH][W(NC_6F_5)F_5]$

For Table of Contents only.